Supporting Information

A Sensitive Lateral Flow Test Strip Sensor for Visual Detection of Acid Red 18 in Food Using Bicentric-Emission Carbon Dots

Houwen Hu[a,1], Zewei Chen[b,1], Tingting Li[a], Linfan Wang[a], Haoming Xing[a], Guoqiang Guo[a,c], Gang Wang[a,d,*], Da Chen[a, *]

[a]Department of Microelectronic Science and Engineering, School of Physical Science and Technology, Ningbo University, Ningbo 315211, P. R. China.

[b]Department of Electrical and Electronic Engineering, Synchrotron Light Application Center, Saga University, Saga 840-8502, Japan.

[c]Department of Materials Science and Engineering, Shenzhen Key Laboratory of Full Spectral Solar Electricity Generation (FSSEG), Southern University of Science and Technology, Shenzhen 518055, P. R. China.

[d]National Key Laboratory of Materials for Integrated Circuits, Shanghai Institute of Microsystem and Information Technology, Chinese Academy of Sciences, Shanghai 200050, P. R. China.

*Corresponding author:

E-mail address: gangwang@nbu.edu.cn (G. Wang); chenda@nbu.edu.cn (D. Chen)

Houwen Hu and Zewei Chen contributed equally to this work.

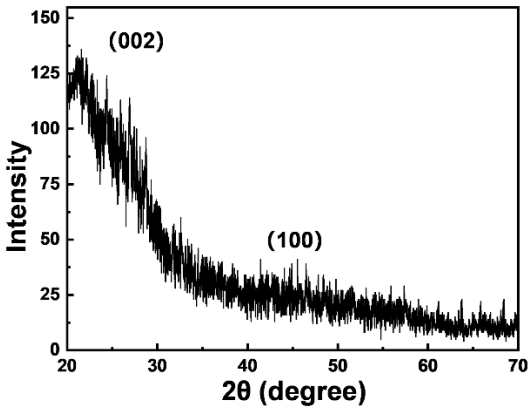

Fig. S1 XRD pattern of N-CDs.

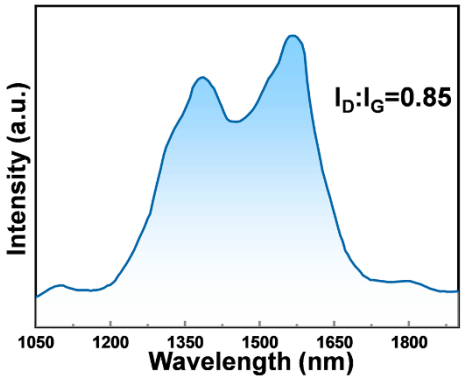

Fig. S2 Raman pattern of N-CDs.

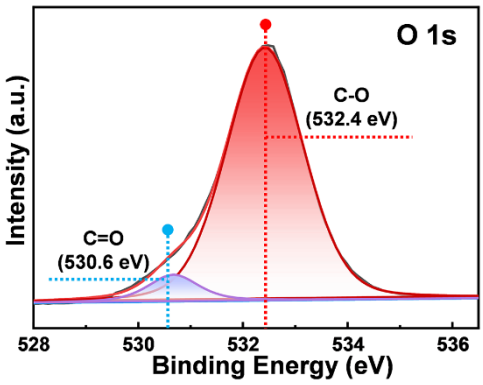

Fig. S3 High-resolution XPS spectrum of O 1s.

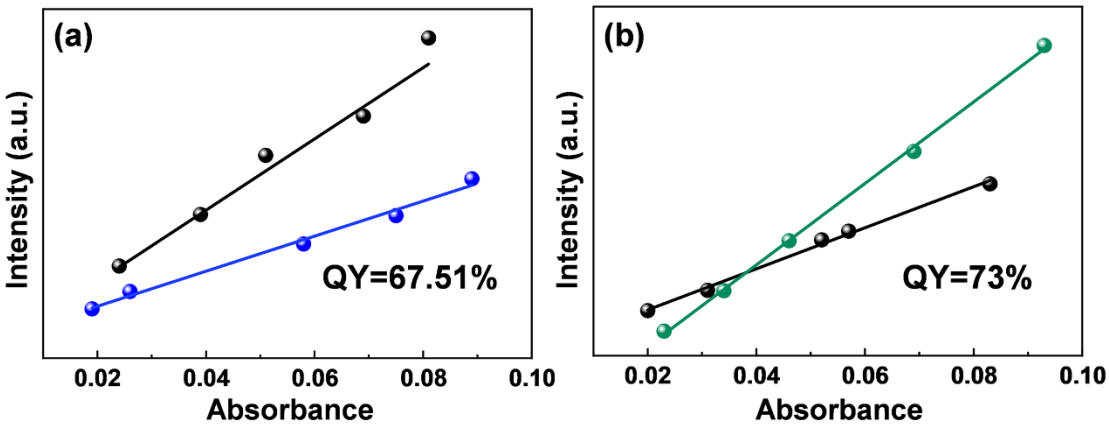

Fig. S4 The linear relationship between 425 nm (a) and 541 nm (b) fluorescence integrated intensity and optical density from the absorbance of N-CDs and Rhodamine B.

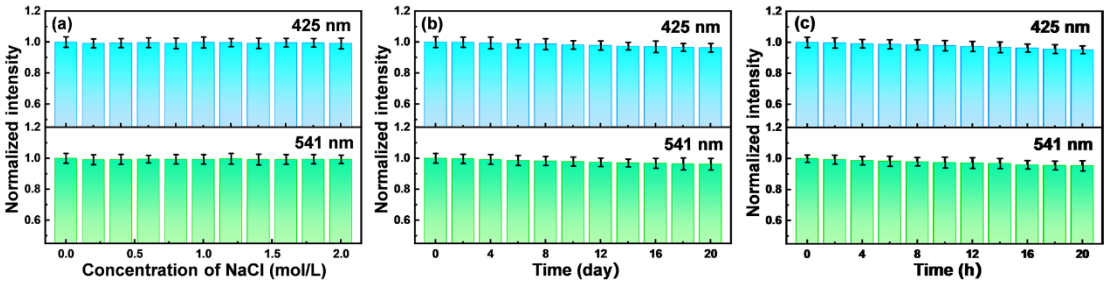

Fig. S5 Fluorescence stability of N-CDs under different concentrations of NaCl (a), storage time in daylight (b) and ultraviolet light (c).

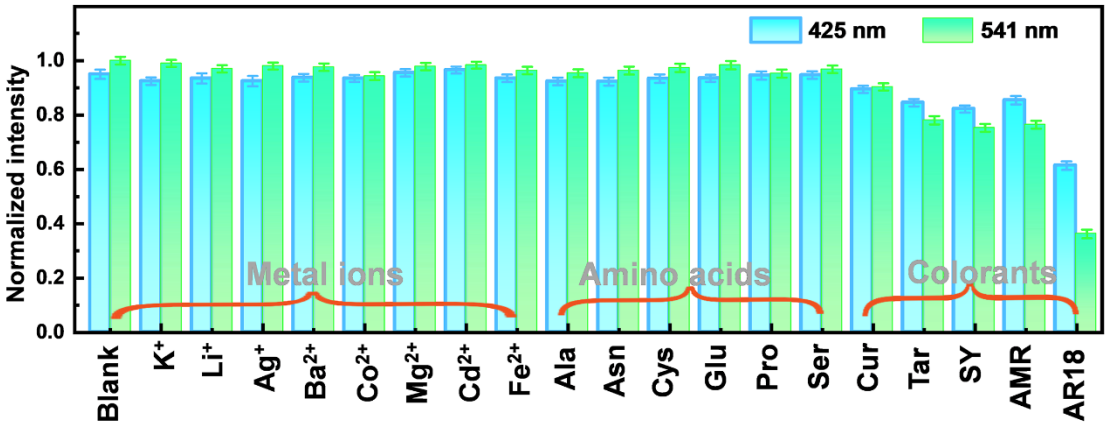

Fig. S6 Selectivity of N-CDs. The concentration of interferent is 100 μM.

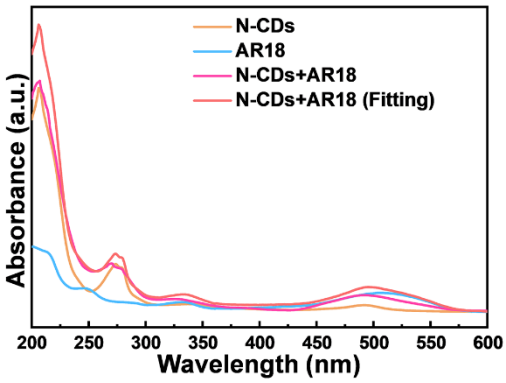

Fig. S7 UV-vis absorption spectra of N-CDs, AR18, the mixture of N-CDs and AR18 and the fitting curve of the mixture.

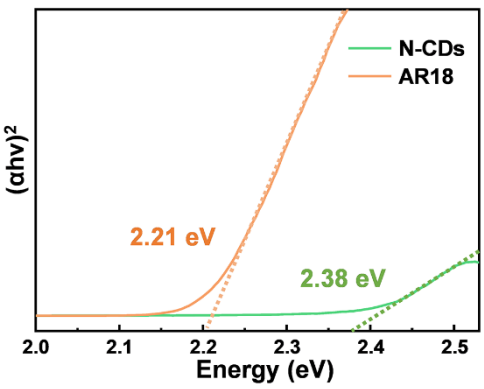

Fig. S8 Tauc plots of N-CDs (orange line) and AR18 (green line).

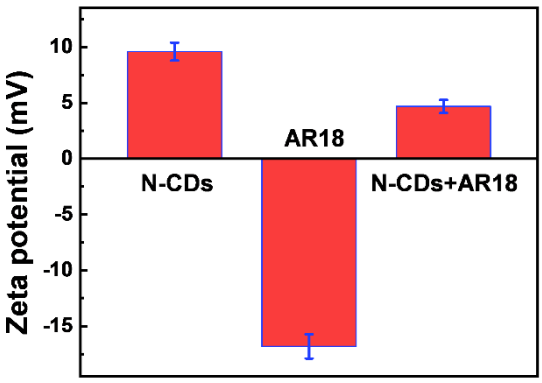

Fig. S9 Zeta potential of AR18, N-CDs and N-CDs+AR18.

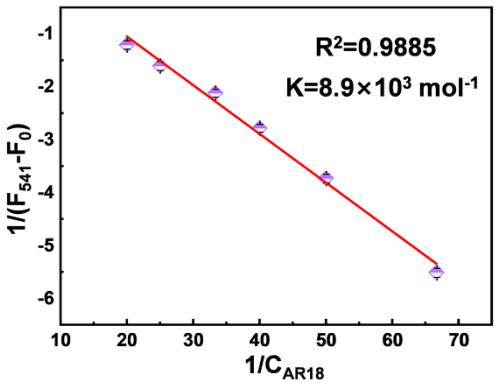

Fig. S10 Benesi-Hildebrand plot of N-CDs upon the addition of AR18.

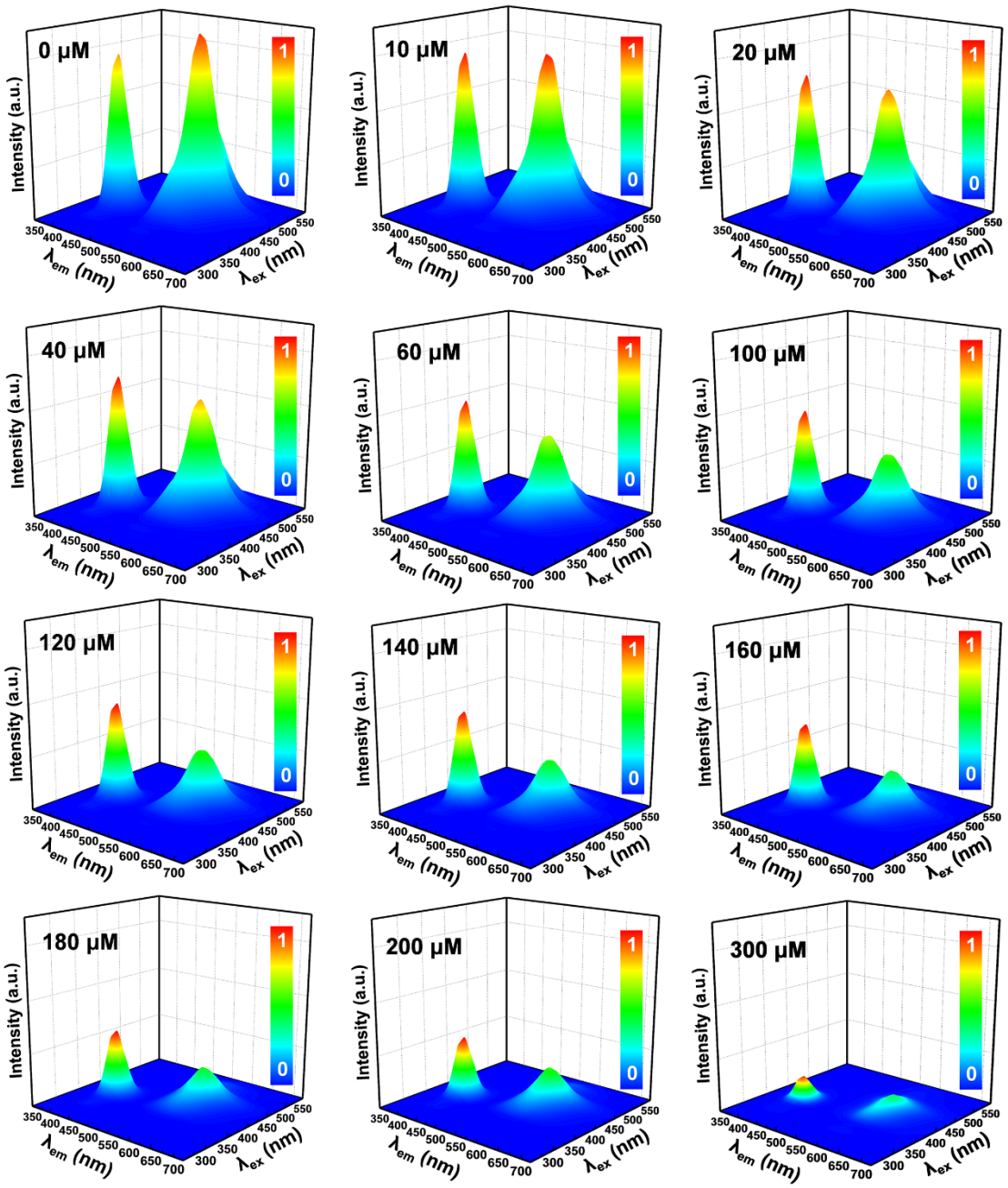

Fig. S11 Normalized 3D fluorescent matric scanning map of N-CDs with different concentrations of AR18.

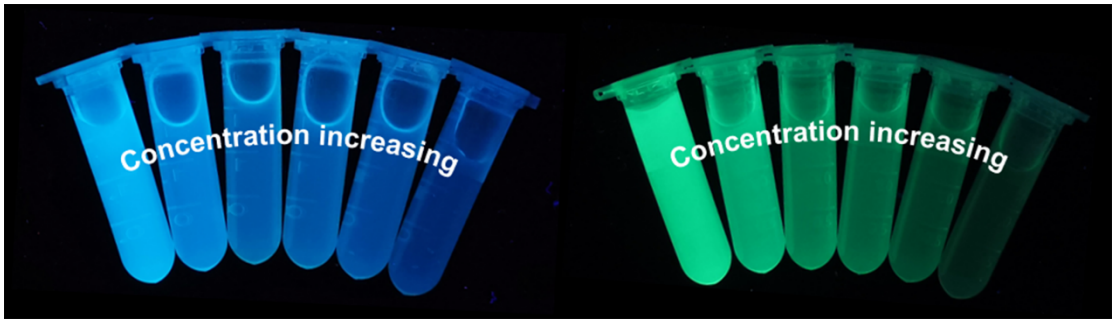

Fig. S12 The images of N-CDs with different concentration of AR18 under UV light of 365 nm (left) and 470 nm (right).

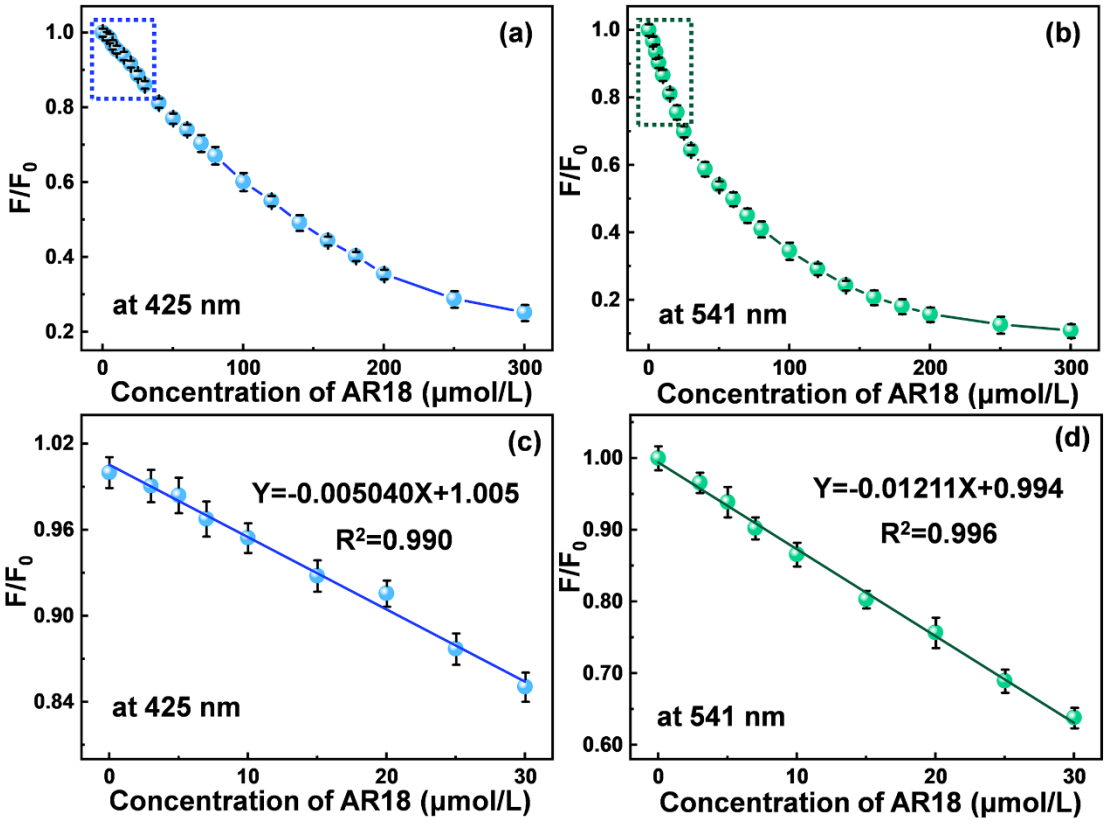

Fig. S13 The relationship between fluorescence intensity ratio (F/F_0) and the concentration of AR18 under the emission wavelength of 425 nm (a) and 541 nm (b). Linear fitting between F/F_0 and the concentration of AR18 under the emission wavelength of 425 nm (c) and 541 nm (d).

Fig. S14 The solution flow on the LFTS sensing platform.

Table S1. Comparations among different detection methods of AR18.

Methods		Analyte	Materials	Linear Range (μM)	LOD (μM)	Ref.
SERS	-	AR18	UiO-66（NH_2）@Au	1.65-82.7	0.664	1
SERS	-	AR18	AuNPs	5-500	5	2
HPLC	-	AR18	-	1.65-33.09	0.414	3
HPLC-UV	-	AR18	-	0.165-16.54	0.0993	4
Fluorescence	Single fluorescence	AR18	F-SiQDs	1-100	0.33	5
Fluorescence	Ratiometric fluorescence	AR18	Fan, N-CDs	20-55	0.0548	6
Fluorescence	3D-ratiometric fluorescence	AR18	N-CDs	0.0539-30	0.0539	This work

References

1. L. Wu, H. Pu, L. Huang, D. Sun, *Food Chem.*, 2022, **328**, 127105.

2. X. Tian, Z. Fan, *Spectrochim. Acta A*, 2012, **96**, 600-604.

3. M. Khanavi, M. Hajimahmoodi, A. Ranjbar, M. Oveisi, M. Ardekani, G. Mogaddam, *Food Anal. Method.*, 2012, **5**, 408-415.

4. S. Dixit, S. Khanna, M. Das, *J. AOAC INT.*, 2010, **93**, 1503-1514.

5. Y. Liu, M. Zan, L. Cao, J. Peng, P. Wang, X. Pang, Y. Zhang, L. Li, Q. Mei, W. Dong, *Microchem. J.*, 2022, **179**, 107453.

6. Y. Tu, Z. Liu, L. Jiang, Y. Xiang, F. Song, L. Meng, X. Ji, L. Yuan, *Dyes Pigm.*, 2023, **210**, 111024.